Macromolecules

Article

pubs.acs.org/Macromolecules

Synthesis, Morphology, and Optical and Electrochemical Properties of Poly(3-hexylthiophene)-*b*-poly(3-thiophene hexylacetate)

Chun-Chih Ho,[†] Yu-Cheng Liu,[‡] Shih-Hsiang Lin,[†] and Wei-Fang Su*[,†,‡]

[†]Department of Materials Science and Engineering, National Taiwan University, Taipei 10617, Taiwan

[‡]Institute of Polymer Science and Engineering, National Taiwan University, Taipei 10617, Taiwan

Supporting Information

ABSTRACT: A series of all-conjugated diblock copolythiophenes of poly(3-hexylthiophene)-*b*-poly(3-thiophene hexylacetate) (P3HT-*b*-P3THA) were synthesized via modified sequential Grignard metathesis polymerization. The living P3HT was formed first, then reacting with the monomer of P3THA. By using 2-bromo-3-hexyloxycarbonylmethylene-5-iodothiophene instead of dibromo monomer in metal exchange reaction and by controlling the polymerization temperature relatively low at 16−20 °C, the reaction between carboxylate group and Grignard reagent can be minimized and the polymerization can be controlled; low PDI (<1.3), high regioregularity (>95%), and well-controlled block ratios of block copolymer were obtained. The introduction of carboxylate group in the side chain of one of the monomers, and controlling the side-chain length difference by only three atoms between two monomers, there are profound effects on the optical and electrochemical properties and morphologies of the block copolymers. The electron-withdrawing carboxylate causes the absorption maximum of copolymer in solution to be blue-shifted from that of pristine P3HT, and the extent of blue shift is increased monotonically with increasing the molar ratio of P3THA. However, in thin film, the intermolecular $\pi-\pi$ stacking plays a role in the absorption behavior of copolymer which decreases the extent of blue shift. The HOMO level of the copolymer is lowered by 0.38 eV from that of P3HT due to the presence of P3THA block. The crystalline structure of the copolymer can be controlled according to the molar ratio of each block. Crystalline−amorphous, crystalline−crystalline, and cocrystalline structures are observed in the bulk samples when the block molar percentage of P3THA is increased from 22, 40, to 50 and higher, respectively. Microphase separation is clearly present in the thin film fabricated from the copolymer containing crystalline−amorphous and crystalline−crystalline structures. The observation of various crystalline structures in a single type of all-conjugated diblock copolymer is very significant and provides a new approach to simultaneously manipulate the optical and electronic properties and nanostructures of conducting polymers by simply changing their compositions.

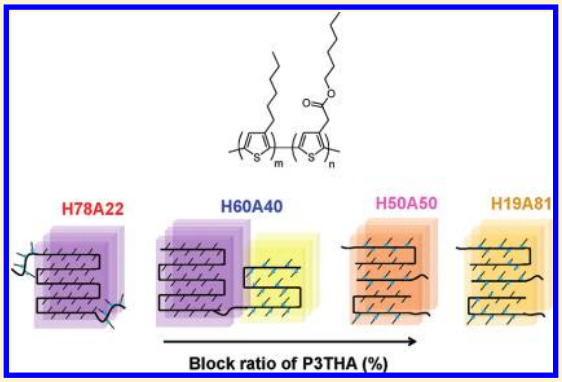

INTRODUCTION

All-conjugated polymers have received great attention in the past decade because of their high potential and promising applications in organic photovoltaic cells (OPVs),[1,2] organic field-effect transistors (OFETs),[3−5] organic chemical sensors,[6] and organic light-emitting diodes (OLEDs).[7] It is very important to control the morphologies of conducting polymers in nanoscale to achieve high performance in the application of optoelectronics.[8−11] To precisely manipulate the nanostructures, one good strategy is to employ block copolymers (BCPs) composed of semiconducting polymer with exceptional electronic properties such as poly(3-alkylthiophene)s (P3AT). BCPs are well-known to have the capability to self-organize into a variety of nanostructures, driven by factors of immiscibility or the crystallinity difference between the two blocks.[12,13] Synthesis and self-assembly of rod−coil BCPs containing a semiconducting block and an insulating block have been extensively investigated.[14−16] We have demonstrated poly(3-hexylthiophene)-*b*-poly(2-vinylpyridine) (P3HT-*b*-P2VP)[14] and poly(diethylhexyloxy-*p*-phenylenevinylene)-*b*-poly(methyl methacrylate) (DEH-PPV-*b*-PMMA)[15] are able to self-assemble into lamellar, cylinder, and spherical structures as increasing the coil fraction. The insulating coil blocks indeed promote the self-assembly and mechanical properties of the copolymer. However, these insulating blocks deteriorate the electronic properties of polymer. McCullough et al. have shown the mobility of OFET fabricated from poly(3-hexylthiophene)-*b*-poly(methyl acrylate) (P3HT-*b*-PMA) decreases as increasing the content of PMA.[17,18] Thus, there is a need to develop all-conjugated BCPs for polymer based high-performance optoelectronic and electronic devices.

Recently, P3ATs-based BCPs have been reported due to their high charge mobility, facile, and versatile synthesis.[19−25] P3ATs-based BCPs exhibit three categories of crystalline

Received: September 25, 2011
Revised: December 19, 2011
Published: December 28, 2011

structures: crystalline−amorphous, crystalline−crystalline, and cocrystalline. Poly(3-hexylthiophene)-*b*-poly(3-phenoxymethylthiophene) (P3HT-*b*-P3PT)[26] and poly(3-hexylthiophene-*b*-poly(3-(2-ethylhexyl)thiophene) (P3HT-*b*-P3EHT)[27] have been synthesized and show crystalline−amorphous structure. The formation of this structure is mostly caused by the large difference in crystallinity between two blocks. The crystalline−crystalline structure is revealed while the crystallization rate of two blocks is similar such as poly(3-butylthiophene)-*b*-poly(3-octylthiophene) (P3BT-*b*-P3OT),[28] poly(3-butylthiophene)-*b*-poly(3-dodecylthiophene) (P3BT-*b*-P3DDT),[29] poly(3-hexylthiophene)-*b*-poly(3-dodecylthiophene) (P3HT-*b*-P3DDT),[29] and poly(3-hexylthiophene)-*b*-poly(3-cyclohexylthiophene) (P3HT-*b*-P3cHT).[24] Ge et al. reported that by controlling the alkyl side-chain length different by two carbon atoms to improve the structure similarity, the cocrystalline structure can be observed in poly(3-butylthiophene)-*b*-poly(3-hexylthiophcne) (P3BT-*b*-P3HT).[29] Nevertheless, none of these BCPs as above-mentioned have shown the effect of block ratio on the formation of various crystalline structures in one single type of all-conjugated diblock copolymer.

The long-term air stability of conducting polymer is a desired property for optoelectronic application. It can be improved by lowering the highest occupied molecular orbital (HOMO) of conducting polymer. The HOMO energy level of polythiophene derivatives can be lowered by diminishing the effective conjugation length from the constrained delocalization. Copolymers of thiophene with thieno[2,3-*b*-]thiophene,[30] fluorene,[31] and naphthalene[32] have shown to have improved environmental stability but higher band gap. Another strategy to lower the HOMO energy level is the incorporation of electron-withdrawing substituents on the polymer backbone. Polythiophenes composed of electronegative carboxylate substituents can effectively increase their oxidative doping stability by lowering the HOMO energy level of conventional polythiophenes about 0.3−0.5 eV.[33−36] Moreover, the carboxylate group can be easily converted into carboxylic acid via hydrolysis. The thus-obtained functionalized group enables the interface interaction between the polymer and inorganic substances and further enhances the interfacial charge-transfer efficiency.[37−40]

Herein, we have synthesized a series of all-conjugated diblock copolythiophenes, poly(3-hexylthiophene)-*b*-poly(3-thiophene hexylacetate) (P3HT-*b*-P3THA), with well-controlled molecular weight and low PDI (<1.3) via modified sequential Grignard metathesis polymerization (GRIM).[28,41] Their optical and electrochemical properties, crystalline behaviors, and nanoscale phase separation were investigated. Our study revealed that optical and electrochemical properties in solid state are attributed to the specific block. Crystalline−amorphous and crystalline−crystalline structures of these BCPs are observed at low 3THA molar fraction (<50%), whereas cocrystalline structures appeared as the 3THA fraction is larger than 50%. Distinct microphase separation is present for the copolymer with 3THA molar fraction is less than 50%.

EXPERIMENTAL SECTION

Materials. 3-Bromothiophene (98%), 3-thiopheneacetic acid (98%), magnesium, 1-bromohexane (98%), 1-hexanol (98%), *N*-bromosuccinimide (98%), iodine (98%), iodobenzene diacetate (98%), isopropylmagnesium chloride (2.0 M solution in THF) (*i*-PrMgCl), Ni(dppp)Cl_2 (99%), and Ni(dppe)Cl_2 (99%) were purchased from Acros and used without further purification. *N*-Butylammonium perchlorate (Bu_4NClO_4) was recrystallized twice from ethanol. THF and ethyl ether for reaction were dried with Na/benzophenone before used. Acetonitrile was dried over CaH_2 and distilled prior to use. The monomers, 2,5-dibromo-3-hexylthiophene (DBHT) and 2-bromo-3-hexyloxycarbonylmethylene-5-iodothiophene (BHOCMIT), were prepared according to the literature.[41,42]

Synthesis of Poly(3-hexylthiophene)-*b*-poly(3-thiophene hexylacetate) Block Copolymers (P3HT-*b*-P3THA). The synthetic conditions of the P3HT-*b*-P3THAs in this work were optimized according to the previous studies[28,41] and also used to synthesize the P3HT and P3THA homopolymers. In general, two 250 mL round-bottom flasks were dried by heating under reduced pressure. When those flasks are cooled to room temperature, DBHT and BHOCMIT were respectively placed in these flasks. Both monomers were evacuated under reduced pressure to remove moisture and oxygen. After dried THF was added, these solutions were cooled down to 0 °C. 2 M *i*-PrMgCl in THF (1.1 equiv) was then added into the DBHT solution. Thirty minutes later, 2.0 mol % Ni(dppe)Cl_2 catalyst was added into the solution at 0 °C and then warmed up to 25 °C for 30 min. Meanwhile, BHOCMIT solution was also reacted with 1.1 equiv of *i*-PrMgCl at 0 °C for 30 min. This Grignard exchanged monomer was introduced via a cannula after the polymerization of the first block was complete. The polymerization of the block copolymer was allowed to proceed at 16−20 °C for another 5 h, and the reaction was then quenched with 5 M HCl solution. The copolymers were purified using Soxhlet extraction with following solvents: methanol, acetone, and hexane in sequence. In this study, the compositions of copolymers are controlled by the feed molar ratio of DBHT:BHOCMIT as follows: 70:30, 53:47, 47:53, and 35:65.

^{1}H Nuclear Magnetic Resonance (^{1}H NMR). The chemical structures and compositions of all synthesized polymers were determined by ^{1}H NMR spectra. These NMR spectra were recorded by a Bruker Avance 400 MHz and $CDCl_3$ was used as solvent.

Gel Permeation Chromatography (GPC). The molecular weight and molecular weight distribution of all synthesized polymers were determined using a Waters GPC (Breeze system). The system was equipped with two Waters Styragel columns (HR3 and HR4E), a refractive index detector (Waters 2414), and a dual-wavelength absorbance detector (Waters 2487). The apparatus was calibrated using polystyrene standards (Waters) and THF used as an eluent at 35 °C.

UV−vis Absorption Spectrometer. The optical properties of all synthesized polymers were characterized by UV−vis absorption spectrometer. UV−vis absorption spectra were recorded by a Perkin-Elmer Lambda 35 UV/vis spectrometer. For the solution state measurement, samples were dissolved in chlorobenzene with concentration of ~10^{-6} M. The samples for the solid state study were prepared by spin-coating on quartz substrate from 10 mg/mL chlorobenzene (CB) solution and subsequently annealed at 150 °C for 15 min.

Cyclic Voltammeter (CV). The highest occupied molecular orbital (HOMO) and the lowest unoccupied molecular orbital (LUMO) of all synthesized polymers were determined by cyclic voltammeter (CH Instrument 611B potentiostat/galvanostat system). Samples were spin-coated from 10 mg/mL CB solution onto ITO substrate and then annealed at 150 °C for 15 min. The substrate, platinum, and silver wire were used as working electrode, counter electrode, and reference electrode, respectively. The electrolyte was prepared by dissolving Bu_4NClO_4 in dried acetonitrile into a 0.1 M solution. All measurements were calibrated using ferrocene (Fe) as the standard, and each scan was proceeded at the scan rate of 100 mV/s.

Wide-Angle X-ray Scattering (WAXS). WAXS experiment was performed on the beamline 13A1 or 17A1 of the National Synchrotron Radiation Research Center (NSRRC), Taiwan. Samples were prepared from CB solution (10 mg/mL) and filled it into a thick washer attached with a kapton sheet. After the solvent was completely evaporated, the samples were annealed at 150 °C for 15 min.

Differential Scanning Calorimetry (DSC). A TA Instruments Q100 DSC was used to probe thermal transitions of polymers. Samples were prepared by CB solution casting directly into DSC pans and then allowing the solvent to evaporate slowly. The samples were

Scheme 1. Synthetic Routes of Poly(3-hexylthiophene)-*b*-poly(3-thiophene hexylacetate) Diblock Copolymer (P3HT-*b*-P3THA)

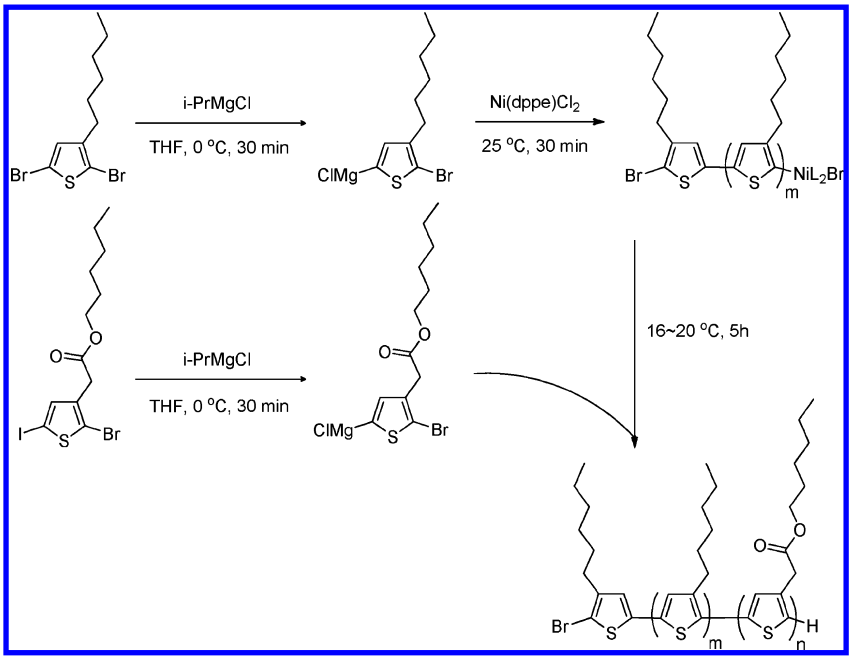

annealed at 150 °C for 15 min prior to DSC analysis. During DSC analysis, samples were reheated to 270 °C at a rate of 5 °C/min.

Atomic Force Microscopy (AFM). The microphase separation of the thin films was characterized by atomic force microscopy (DI Nanoscope III AFM instrument). The samples were prepared by spin-coating 10 mg/mL CB solution on silicon wafer, followed by annealing at 150 °C for 15 min.

RESULTS AND DISCUSSION

Synthesis of P3HT-*b*-P3THAs. Although the living character of GRIM polymerization for synthesizing diblock copolythiophenes with all alkyl side chain[22,29] and functionalized side chain[26,43] has been described, the synthesis of well-defined and carboxylate functionalized diblock copolythiophenes has not been reported. A series of P3HT-*b*-P3THA diblock copolymers with different compositions were synthesized using modified sequential GRIM method, as illustrated in Scheme 1. The type of the monomer, reaction sequence, and temperature are carefully designed and optimized.

Initially, we used dibrominated carboxylate functionalized monomers to obtain P3THA at room temperature, but the molecular weight and molecular weight distribution were uncontrollable. Instead, by replacing one reactive bromine of the carboxylated funcationalized monomers with iodine, the side reaction of carboxylate group with the Grignard reagent was diminished during the magnesium–halogen exchange reaction.[41] The activated monomers were dramatically deprotonated in a short period while the reaction temperature was raised above 20 °C. Hence, it is crucial to control temperature in both metal-exchange stage (0 °C) and polymerization stage (16–20 °C). Because of the lower reactivity of the carboxylate functionalized 3THA monomers[41] as compared to 3HT monomers,[44] we grew P3HT block first in living state and then grew P3THA subsequently by reacting the living P3HT with 3HTA. The amount of 3HTA used was in excess in the feed molar ratio to compensate its lower reactivity. The extent of excess is increased with increasing P3THA ratio. GPC profiles of the first block of P3HT and P3HT-*b*-P3THA are shown in Figure 1 (rest of compositions is shown in Figure S1 of the Supporting Information). The prepared P3HT is in unimodal shape and narrow polydispersity. After adding the activated 3THA monomers, the peak shifts to higher molecular weight and remains unimodal shape, indicative of the formation of P3HT-*b*-P3THA diblock copolythiophene. Thus, well-controlled molecular weight ranged from 16 923 to 24 416, PDI below 1.3; four different molar ratios of diblock copolythiophenes were obtained, and their molecular characteristics are summarized in Table 1. We have used the symbol of HXXAYY to name the copolymer. H is P3HT segment and A is P3THA segment while XX and YY represent their molar ratio, respectively. For example, H78A22 is a block copolymer containing 78 mol % of P3HT and

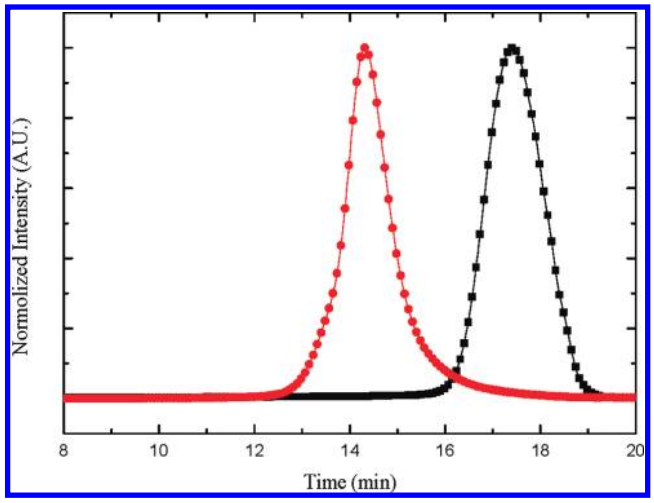

Figure 1. Representative GPC profiles of the first block of P3HT homopolymer (black square) synthesized via the modified GRIM method and P3HT-*b*-P3THA (H19A81) diblock copolymer (red circle) subsequently grown after introducing the activated 3THA monomers.

dx.doi.org/10.1021/ma202164d | *Macromolecules* 2012, 45, 813–820

Table 1. Summary of Molecular Properties of P3HT, P3THA, and P3HT-*b*-P3THA

polymer	denotation	feed molar ratio	3HT:3THA[a]	M_w	PDI
P3HT		100:0	100:0	23 369	1.17
P3THA		0:100	0:100	17 857	1.30
P3HT-*b*-P3THA	H78A22	70:30	78:22	16 847	1.14
	H60A40	53:47	60:40	24 416	1.18
	H50A50	47:53	50:50	16 923	1.21
	H19A81	35:65	19:81	18 677	1.28

[a]Molar ratio determined by ^{1}H NMR.

22 mol % of P3THA. This symbol system is used throughout the study.

The compositions of these polymers were determined from their ^{1}H NMR spectra (Figure S2). Singlet peaks observed at 6.98 and 7.18 ppm are respectively attributed to the thiophene proton on P3HT segment and P3THA segment. Peaks at 3.81 and 4.16 ppm are belonging to the methylene protons neighboring to the thiophene rings and the oxygen atoms, respectively, of the side chains of P3THA. A methylene proton attributed to the side chain of P3HT segment is observed at 2.81 ppm. The regioregularity[45] and molar ratio of P3HT-*b*-P3THA diblock copolymers were estimated from the proton on thiophene ring and that adjacent to thiophene ring of each block. The regioregularity of each block is more than 95%, suggesting high regioselectivity is achieved for each block.

Optical and Electrochemical Properties. The optical and electrochemical properties of P3HT-*b*-P3THA diblock copolythiophenes were studied by using UV−vis absorption spectroscopy and electrochemical cyclic voltammetry (CV). In CB solution, the UV−vis spectra of these copolymers show a single absorption maxima which is placed in between that of P3HT (456 nm) and P3THA homopolymers (425 nm), as shown in Figure 2a. The peak is blue-shifted monotonically from 450 to 430 nm as increasing the P3THA fraction, which means the two blocks are miscible. However, very different features of UV−vis spectra are observed in the thin film samples due to the different crystalline behavior of each block, as shown in Figure 2b. Three characteristic peaks attributed to the intrachain $\pi-\pi^*$ transition (525 nm), the increased conjugation length (560 nm), and the interchain $\pi-\pi$ interaction (600 nm) for P3HT are observed, whereas only one peak at 425 nm is observed for P3THA. It is suggested that P3HT has better structural organization than the P3THA. In block copolymers, two characteristic peaks of 560 and 600 nm are belonging to the increased conjugation length and the interchain $\pi-\pi$ interaction of polythiophene main chain. The interference effects on the structural organizations are increasing as increasing the P3THA fraction when we compared the normalized intensities of these two peaks among the copolymers. However, the absorption maximum of P3THA becomes dominate when the molar ratio of P3THA is larger than 50%. It is interesting to note that the absorption maximum of P3THA of copolymer is red-shifted from the pristine P3THA. We speculate that the synergistic effect from P3HT block increases the effective conjugation length of the P3THA block by increasing the P3HT molar ratio and induces cocrystallization between P3THA block and P3HT block. We will discuss these phenomena more in the section of crystalline behaviors.

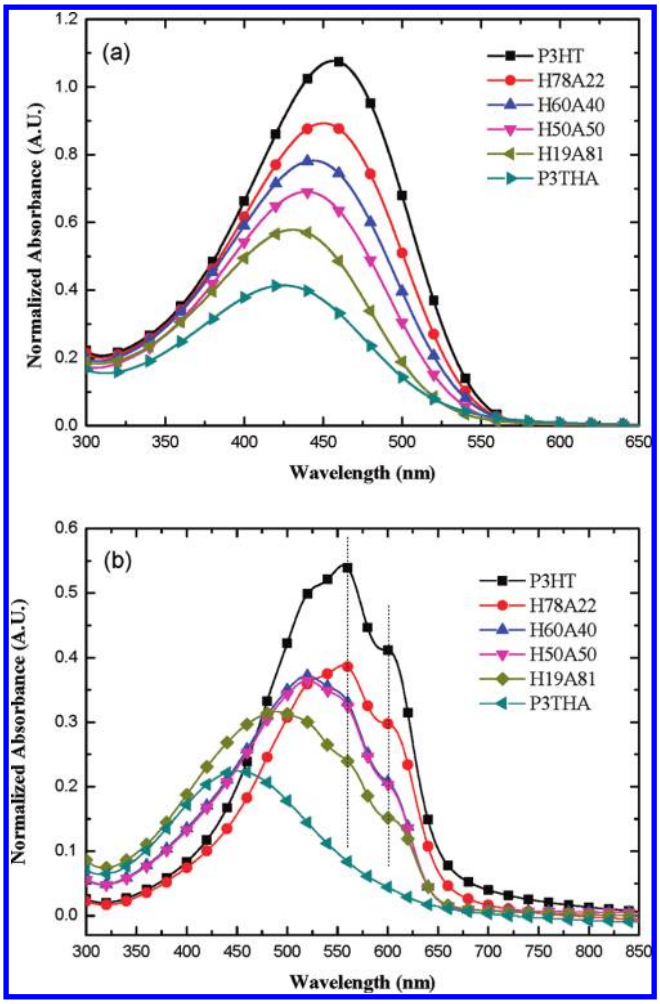

Figure 2. Normalized UV−vis absorption spectra of P3HT-*b*-P3THA diblock copolythiophenes and their homopolymers in (a) solution and (b) film. In film spectra, the dashed lines are assigned to the increased conjugation length peak (560 nm) and the $\pi-\pi$ interaction peak (600 nm).

CV measurements were used to study redox behaviors of the P3HT-*b*-P3THA diblock copolythiophenes. The highest occupied molecular orbital (HOMO) and the lowest unoccupied molecular orbital (LUMO) energy levels from their onset oxidation and reduction potentials were determined, respectively. Figure 3 shows the cyclic voltammograms of P3HT, P3HT-*b*-P3THA, and P3THA. The onsets of oxidation potential (E_{ox}) and reduction potential (E_{red}) for P3THA are shown to be 0.949 and −1.043 V, respectively, while a distinguishable onset E_{ox} of 0.569 V is belonging to P3HT. Comparing to the P3HT, the oxidation potential of P3THA shows an increase of 0.38 V by placing the electron-deficient carboxylate group on the side chain. The HOMO and LUMO energy levels of the polymers were estimated according to the equations of $E_{LUMO} = -e(E_{red} + 4.8)$ (eV) and $E_{HOMO} = -e(E_{ox} + 4.8)$. The E_{LUMO} and the E_{HOMO} of the P3THA are positioned at −3.36 and −5.35 eV, respectively, while the E_{HOMO} of the P3HT is located at −4.97 eV. Interestingly, the E_{LUMO} and the E_{HOMO} of P3THA and P3HT blocks can be clearly identified in all copolythiophenes. The LUMO of P3THA block is lower than the LUMO of P3HT block by 0.3 eV, and the HOMO of P3THA block is lower than the HOMO of P3HT block by 0.38 eV. Herein, the enlargement of band gap in all

dx.doi.org/10.1021/ma202164d | *Macromolecules* 2012, 45, 813−820

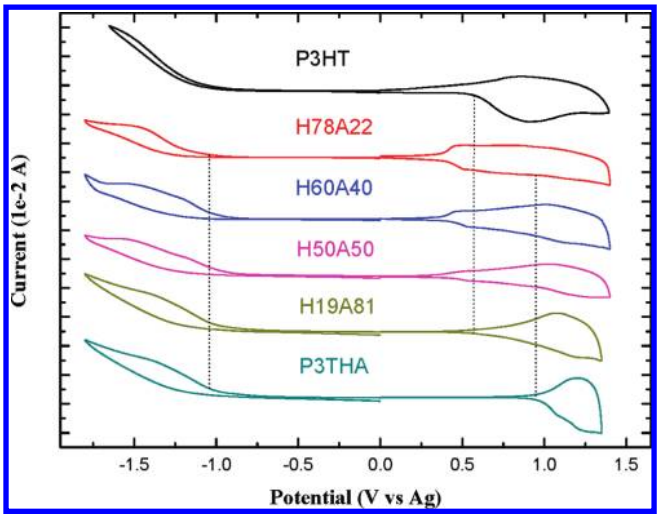

Figure 3. Cyclic voltammograms of P3HT-*b*-P3THA diblock copolythiophenes and their homopolymers. These samples were measured on ITO electrode in acetonitrile solution containing 0.1 M BuN_4ClO_4 at a scan rate of 100 mV/s. Dashed lines are represented as the onset of oxidation or reduction potentials. All curves are offset for clarity.

composition of P3HT-*b*-P3THAs as compared to that of P3HT is less than 0.17 eV calculated by optical band gap and 0.26 eV calculated by electrical band gap. These results suggest that the introduction of carboxylate group on the side chain is a very effective way to lower the E_{HOMO} of alkyl-substituted polythiophene for long-term air stability. For the copolymer having the molar ratio of P3THA ranged from 22 to 81%, the individual redox properties of each block is still remained which shows the characteristic of block copolymer.

Crystalline Behaviors. In order to investigate the crystalline behaviors of the P3HT-*b*-P3THA diblock copolythiophenes, WAXS and DSC measurements were performed. The study of crystalline behaviors of P3HT and P3THA was included for the purpose of comparison. Figure 4 reveals a lamellar structure for all polymer samples according to their characteristic peaks of WAXS. A peak associated with (100) reflection can be clearly observed for all of the samples, and the higher order reflections (*h*00) still can be recognized except for P3THA. Additionally, the peak at 15.8−16.6 nm^{-1} is assigned to the (020) reflection, which corresponds to the $\pi-\pi$ stacking distance of 0.378−0.398 nm and is accompanied by a broad halo resulting from the amorphous side chains. The interlayer d_{100} spacing of copolymers and their corresponding homopolymers are summarized in Table 2. The P3HT should be easier to form crystalline than P3THA because the hexyl side chain is less bulky and shorter than hexyl acetate side chain. Thus, the d_{100} spacing of P3HT is smaller than that of P3THA (16.11 vs 20.17 nm). The d_{100} spacing of the copolymers is in between the d_{100} spacing of P3HT and P3THA except the H19A81. The result again indicates the P3HT and P3THA are miscible. By following the simple mixing rule, the d_{100} spacing of the copolymers is expected to be larger than P3HT and smaller than P3THA. The d_{100} spacing of H19A81 is slight larger than that of pristine P3THA (20.27 vs 20.17 nm) which may be due to the competing crystallization between P3HT and P3THA and results in a less organized crystal. The (100) peak of H60A40 can be resolved into two peaks (see Figure S3) to have two d_{100} spacing values due to the presence of both P3HT crystalline

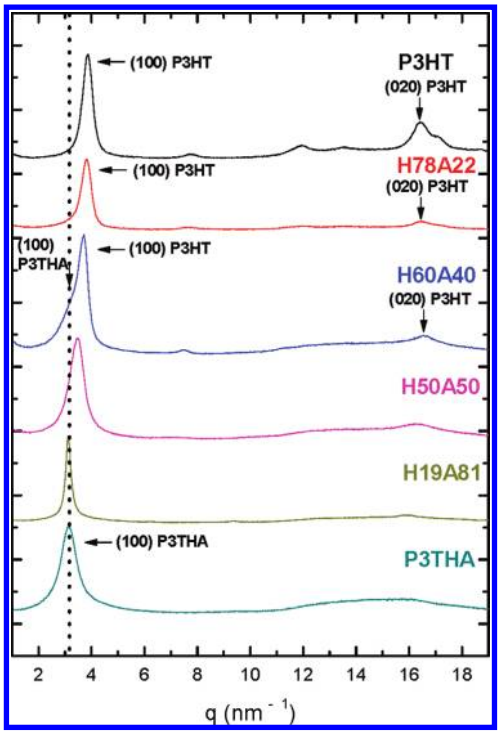

Figure 4. WAXS profiles of P3HT, P3THA, and P3HT-*b*-P3THA diblock copolythiophenes. Dashed line is presented as the (100) plane position of P3THA homopolymer to aid the comparison of the (100) planes of other polymers. All curves are offset for clarity.

Table 2. Summary of WAXS Measurements of P3HT, P3THA, and P3HT-*b*-P3THAs

polymer	d_{100}/nm (q/nm^{-1})	polymer	d_{100}/nm (q/nm^{-1})
P3HT	16.11 (0.39)	H50A50	17.95 (0.35)
H78A22	16.53 (0.38)	H19A81	20.27 (0.31)
H60A40	16.98 (0.37), 20.17 (0.29)	P3THA	20.17 (0.29)

and P3THA crystalline (demonstrate later by variable temperature WAXS study). However, a single (100) peak is observed for H50A50 and H19A81, which suggests the formation cocrystalline structure in the copolymer containing more than 50% molar ratio of P3THA (demonstrated later by variable temperature WAXS study).

Figure 5 shows the DSC thermograms of P3HT-*b*-P3THA diblock copolythiophenes and their homopolymers. The results are summarized in Table 3. For H78A22, only one transition is observed around 226 °C which is close to 235 °C of P3HT. This sample is likely to form microphase separation due to different crystalline behavior between P3HT and P3THA. The melting point of H78A22 is lower than that of P3HT because the P3THA segment is too short to form crystal and is dispersed randomly around P3HT crystal. For H60A40, two distinct transitions are observed at 138 and 216 °C for P3THA segment and P3HT segment, respectively. As the result, we can speculate that each segment of H60A40 is long enough to form its own crystalline domain with microphase separation. Thus, a crystalline−crystalline structure is formed. For H50A50 and H19A8, they show only a broad peak in the DSC thermograms which may exhibit a cocrystalline behavior. The results suggest that the crystalline structure of block copolymer is varied with changing the

dx.doi.org/10.1021/ma202164d | *Macromolecules* 2012, 45, 813−820

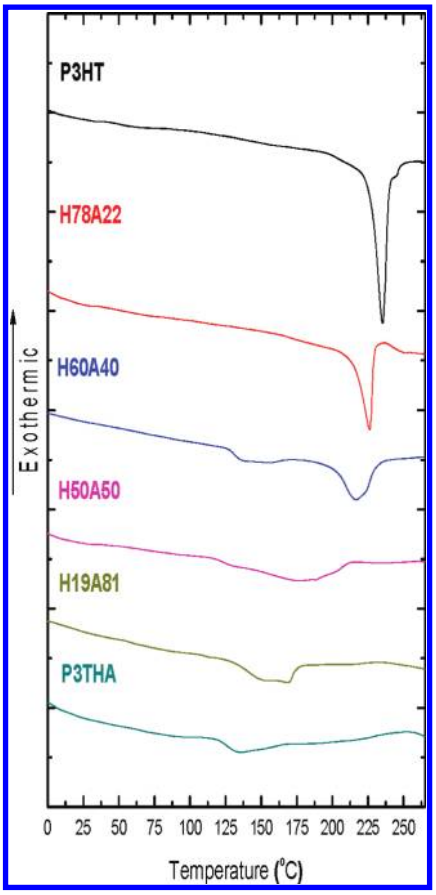

Figure 5. DSC thermograms of P3HT, P3THA, and P3HT-*b*-P3THAs.

Table 3. Results of DSC Measurements of P3HT, P3THA, and P3HT-*b*-P3THA

polymer	T_m/°C	polymer	T_m/°C
P3HT	235	H50A50	175
H78A22	226	H19A81	168
H60A40	138, 217	P3THA	135

molar ratio of two blocks as sketched in Figure 6. However, it is puzzled to see that two transitions are preent in the DSC

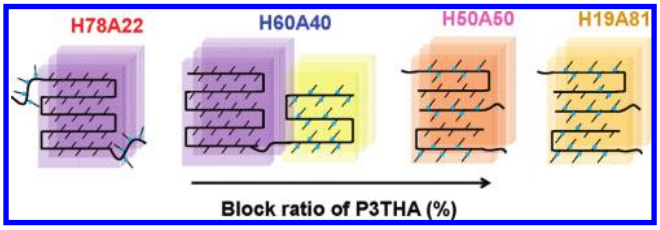

Figure 6. Schematic illustrations of crystalline structures in P3HT-*b*-P3THA diblock copolythiophenes. Blue spot is assigned as the carboxylate group on the P3THA side chain. The purple, yellow, and brown colors are assigned as P3HT crystalline structure, P3THA crystalline structure, and cocrystalline structure of P3HT and P3THA polymers. These copolythiophenes form various crystalline structures with increasing the block ratio of P3THA as follows: crystalline–amorphous, crystalline–crystalline, and cocrystalline structures.

thermogram of H60A40; only one peak with a slightly shoulder at lower-q region is observed in the WAXS scan. Thus, we performed variable temperature WAXS measurements to further confirm the crystalline behavior which is affected by changing the molar ratio of the copolymer, as shown in Figure 7.

In Figure 7a, the (100) reflection of the H78A22 was completely disappeared while the temperature was raised above 240 °C. This transition temperature is close to that of P3HT at 235 °C in the DSC study. Together with the result of similar d_{100} spacing of H78A22 to that of P3HT, we can confirm the crystalline P3HT is present in H78A22. For H60A40 (Figure 7b), the intensity of the shoulder at low-q region, its location is similar to the (100) reflection of P3THA, decreases as increasing the temperature. Until heating to 150 °C, the shoulder completely disappeared with no reduction of the primary peak, indicative of this melted crystal is attributed to the P3THA block. Upon further heating to 190 °C, the intensity of the peak attributed to P3HT block starts to decrease, and finally the peak completely disappeared after heating above 230 °C. These two transition temperatures are in good agreement with the DSC study and are consistent with the deconvolution of the (100) peak (Figure S3). To deconvolute the (100) peak, the peak profile of P3HT block at 150 °C was used as the calculation basis; the peak position of P3THA was set, and thus the desired peak profile assumed to be the P3THA block can be extracted. The breadth of the calculated peak of P3THA block is similar to that of P3THA. Scrutinizing the results of transition temperatures, d_{100} spacing, and peak deconvolution, the crystalline–crystalline structure is deduced for H60A40. When the P3THA fraction is above 50%, the copolythiophenes show different crystalline behaviors. Both H50A50 and H19A81 exhibit only one peak until reaching their respective transition temperatures (Figure 7c,d). The H19A81 has a lower melting point (~170 °C) than that of H50A50 (~190 °C) because the higher P3THA fraction in H19A81. The results show similar trend in the DSC study. Note that d_{100} spacing of H50A50 is smaller than that of H19A81, indicative of closer packing and higher melting temperature. Summarizing the results from DSC and variable temperature WAXS measurements, the presence of cocrystalline structure in H50A50 and H19A81 is confirmed.

Microphase Separation. To further study the microphase separation behavior of P3HT-*b*-P3THA, their nanostructures were probed using AFM measurements. Although the height image of H78A22 shows a blurred pattern (Figure 8a), its phase image exhibits distinct nanopatterns with short lamellar-like structure (Figure 8b). The width of the short lamellae is irregular and is in the range of 15–25 nm. Since the P3THA segment of H78A22 is too short to form the crystalline structure, the high crystallinity of P3HT block dominates the nanostructure. When the P3HT fraction is decreased further, the influence from the profound crystallization ability of P3HT block is suppressed during the microphase separation process. A blur height image of H60A40 is also observed (Figure 8c) while its phase image appears clear nanopatterns with lamellar-like structure (Figure 8d). The lamellae are continuous and regular in size (~15 nm). The orientation of lamellae is correlated for 4–5 lamellae per bunch. The light region in the lamellae could be attributed to the crystalline area of the P3HT block, since the P3HT block has higher crystallinity than that of the P3THA block. The result suggests the morphology of H60A40 is dominated by the microphase separation due to the P3THA block is long enough to crystallize and thus prevents the substantially crystallization-driven from the P3HT block. As above-mentioned, when the P3THA fraction is higher than 50%, the copolymers show cocrystallization nature. Indeed, these copolythiophenes show smooth surface without

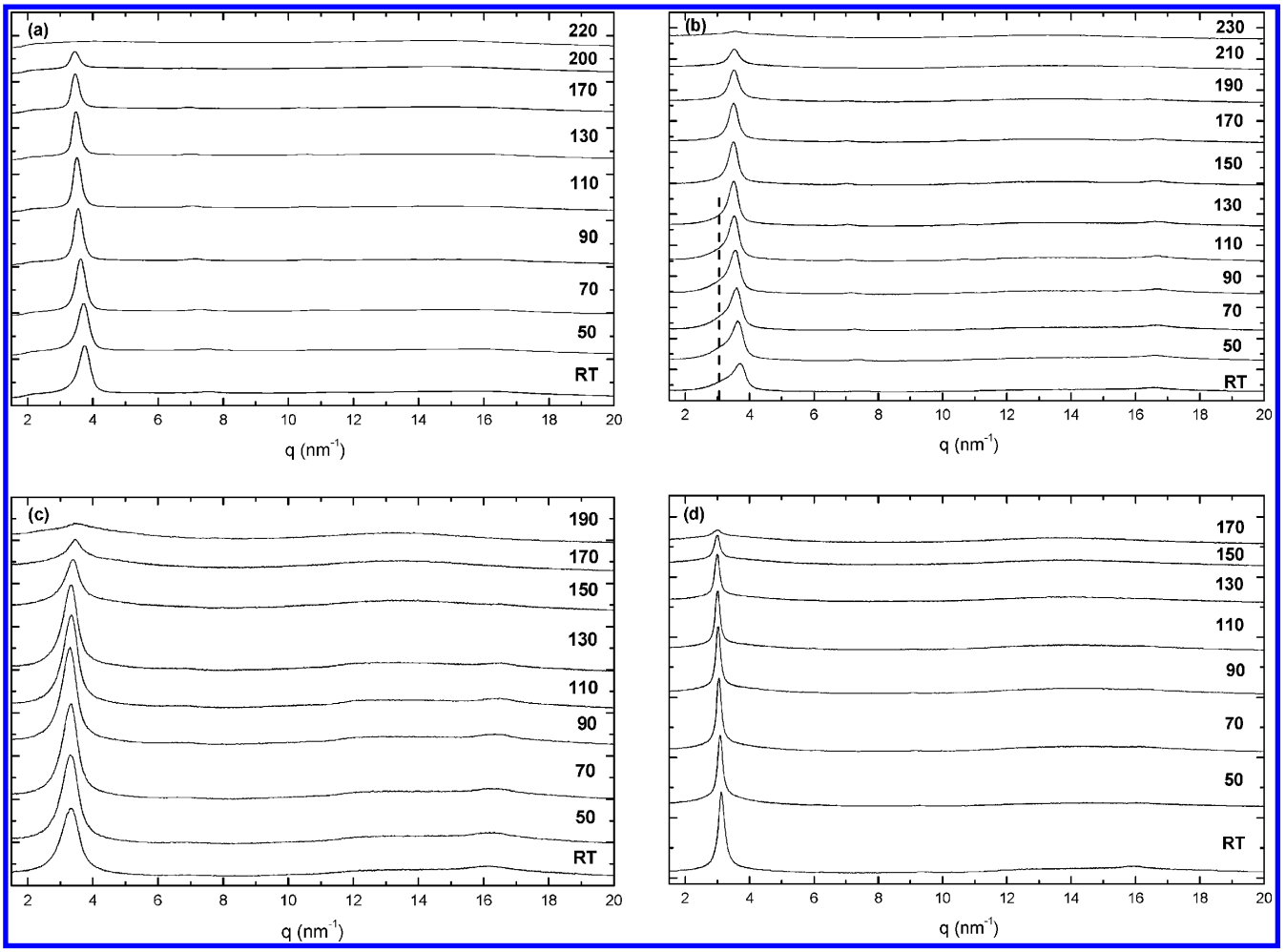

Figure 7. WAXS curves of P3HT-*b*-P3THA diblock copothiophenes at different temperatures. The primary peaks are assigned as (100) plane in (a) H78A22, (b) H60A40, (c) H50A50, and (d) H19A81. Dashed line is used to locate the position of the (100) plane attributed to P3THA homopolymer. Curves are offset for clarity.

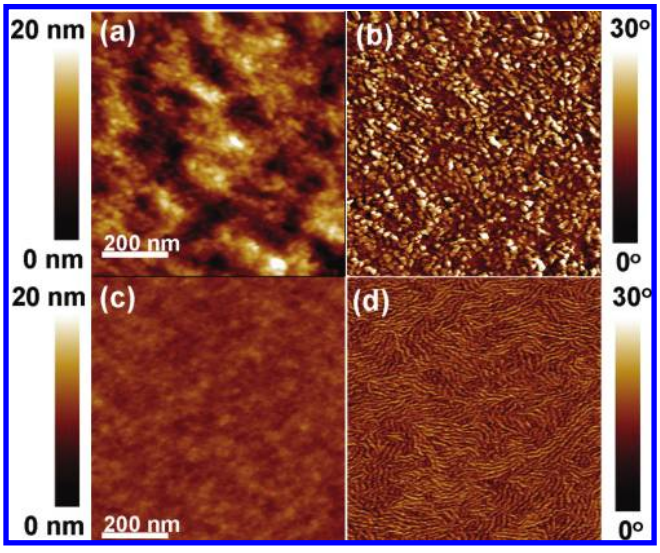

Figure 8. AFM height images and phase images of H78A22 and H60A40 diblock copolythiophenes. While H78A22 (a) and H60A40 (c) both show blur in height images, phase images of H78A22 (b) and H60A40 (d) reveal microphase separation morphologies in nanoscale.

phase contrast (Figure S4) which are similar to the previous reports.[29,46]

CONCLUSION

We have successfully synthesized a series of all-conjugated diblock copolythiophenes P3HT-*b*-P3THA by the modified sequential GRIM method. Through the use of 2-bromo-3-hexyloxycarbonylmethylene-5-iodothiophene and the polymerization at low temperature (16−20 °C), the obtained copolythiophenes have high regioregularity (>95%), well-controlled block ratio, and molecular weight with narrow PDI (<1.3). By introducing the carboxylate group and controlling the blocks with side-chain length difference by only three atoms, profound effects on the optical and electrochemical properties and morphologies of the diblock copolythiophenes are observed. UV−vis absorption spectra show that the absorption maximum of copolymer in solution is blue-shifted monotonically as increasing the molar ratio of P3THA due to the presence of a carboxylate group. Whereas in thin film, the intermolecular $\pi-\pi$ stacking reflected on the absorption behavior of copolymer; thus, the extent of blue shift is decreased. All four P3HT-*b*-P3THA copolymers exhibit lower HOMO level by 0.38 eV from that of P3HT because of the P3THA block. The WAXS and DSC measurements reveal that these block copolythiophenes possess a variety of crystalline structures: crystalline−amorphous, crystalline−crystalline, and cocrystalline with increasing the P3THA fraction. The microphase separation is occurred when the molar ratio of P3THA is less than 50%,

whereas no distinct nanopatterns are observed as the P3THA fraction is higher than 50%. The results of this study give a new insight of manipulating optical and electrochemical properties and nanostructures of conducting block polymer simultaneously by simply adjusting its compositions. Studies of photovoltaic devices and sensors using these block copolymer are in progress.

■ ASSOCIATED CONTENT

Supporting Information

GPC traces and ^{1}H NMR spectra of P3HT-*b*-P3THA diblock copolythiophenes; peak deconvolution of H60A40 in WAXS profile; AFM images of H50A50 and H19A81. This material is available free of charge via the Internet at http://pubs.acs.org.

■ AUTHOR INFORMATION

Corresponding Author

*E-mail: suwf@ntu.edu.tw.

■ ACKNOWLEDGMENTS

We gratefully acknowledge the financial support from the National Science Council of Taiwan (NSC 99-2221-E-002-020-MY3). We also thank the Department of Chemistry of National Taiwan University for the use of their NMR spectrometer. WAXS experimental help provided by Dr. Jey-Jau Lee and Dr. Ching-Yuan Cheng at 17A1 station and Dr. Ming-Tao Lee at 13A1 station of the National Synchrotron Radiation Research Center, Taiwan, is highly appreciated.

■ REFERENCES

(1) Gunes, S.; Neugebauer, H.; Sariciftci, N. S. *Chem. Rev.* **2007**, *107* (4), 1324−1338.
(2) Blom, P. W. M.; Mihailetchi, V. D.; Koster, L. J. A.; Markov, D. E. *Adv. Mater.* **2007**, *19* (12), 1551−1566.
(3) Di, C. A.; Yu, G.; Liu, Y.; Zhu, D. *J. Phys. Chem. B* **2007**, *111* (51), 14083−14096.
(4) Muccini, M. *Nature Mater.* **2006**, *5* (8), 605−613.
(5) Yamashita, Y. *Sci. Technol. Adv. Mater.* **2009**, *10* (2), 024313.
(6) Thomas, S. W.; Joly, G. D.; Swager, T. M. *Chem. Rev.* **2007**, *107* (4), 1339−1386.
(7) Kulkarni, A. P.; Tonzola, C. J.; Babel, A.; Jenekhe, S. A. *Chem. Mater.* **2004**, *16* (23), 4556−4573.
(8) Berresheim, A. J.; Muller, M.; Mullen, K. *Chem. Rev.* **1999**, *99* (7), 1747−1785.
(9) Carroll, D. L.; Reyes-Reyes, M.; Kim, K.; Dewald, J.; Lopez-Sandoval, R.; Avadhanula, A.; Curran, S. *Org. Lett.* **2005**, *7* (26), 5749−5752.
(10) Tao, Y. F.; McCulloch, B.; Kim, S.; Segalman, R. A. *Soft Matter* **2009**, *5* (21), 4219−4230.
(11) Yang, X. N.; Loos, J.; Veenstra, S. C.; Verhees, W. J. H.; Wienk, M. M.; Kroon, J. M.; Michels, M. A. J.; Janssen, R. A. J. *Nano Lett.* **2005**, *5* (4), 579−583.
(12) Bates, F. S.; Fredrickson, G. H. *Phys. Today* **1999**, *52* (2), 32−38.
(13) Lee, M.; Cho, B. K.; Zin, W. C. *Chem. Rev.* **2001**, *101* (12), 3869−3892.
(14) Dai, C. A.; Yen, W. C.; Lee, Y. H.; Ho, C. C.; Su, W. F. *J. Am. Chem. Soc.* **2007**, *129* (36), 11036−11038.
(15) Ho, C. C.; Lee, Y. H.; Dai, C. A.; Segalman, R. A.; Su, W. F. *Macromolecules* **2009**, *42* (12), 4208−4219.
(16) Olsen, B. D.; Segalman, R. A. *Macromolecules* **2005**, *38* (24), 10127−10137.
(17) Sauve, G.; McCullough, R. D. *Adv. Mater.* **2007**, *19* (14), 1822−1825.
(18) Iovu, M. C.; Zhang, R.; Cooper, J. R.; Smilgies, D. M.; Javier, A. E.; Sheina, E. E.; Kowalewski, T.; McCullough, R. D. *Macromol. Rapid Commun.* **2007**, *28* (17), 1816−1824.
(19) Shrotriya, V.; Ouyang, J.; Tseng, R. J.; Li, G.; Yang, Y. *Chem. Phys. Lett.* **2005**, *411* (1−3), 138−143.
(20) Sirringhaus, H.; Brown, P. J.; Friend, R. H.; Nielsen, M. M.; Bechgaard, K.; Langeveld-Voss, B. M. W.; Spiering, A. J. H.; Janssen, R. A. J.; Meijer, E. W.; Herwig, P.; de Leeuw, D. M. *Nature* **1999**, *401* (6754), 685−688.
(21) Yang, H. C.; Shin, T. J.; Yang, L.; Cho, K.; Ryu, C. Y.; Bao, Z. N. *Adv. Funct. Mater.* **2005**, *15* (4), 671−676.
(22) Zhang, Y.; Tajima, K.; Hirota, K.; Hashimoto, K. *J. Am. Chem. Soc.* **2008**, *130* (25), 7812−7813.
(23) Ren, G. Q.; Wu, P. T.; Jenekhe, S. A. *Chem. Mater.* **2010**, *22* (6), 2020−2026.
(24) Wu, P. T.; Ren, G. Q.; Kim, F. S.; Li, C. X.; Mezzenga, R.; Jenekhe, S. A. *J. Polym. Sci., Part A: Polym. Chem.* **2010**, *48* (3), 614−626.
(25) Ren, G. Q.; Wu, P. T.; Jenekhe, S. A. *ACS Nano* **2011**, *5* (1), 376−384.
(26) Ohshimizu, K.; Ueda, M. *Macromolecules* **2008**, *41* (14), 5289−5294.
(27) Zhang, Y.; Tajima, K.; Hashimoto, K. *Macromolecules* **2009**, *42* (18), 7008−7015.
(28) Wu, P. T.; Ren, G. Q.; Li, C. X.; Mezzenga, R.; Jenekhe, S. A. *Macromolecules* **2009**, *42* (7), 2317−2320.
(29) Ge, J.; He, M.; Qiu, F.; Yang, Y. L. *Macromolecules* **2010**, *43* (15), 6422−6428.
(30) Heeney, M.; Bailey, C.; Genevicius, K.; Shkunov, M.; Sparrowe, D.; Tierney, S.; McCulloch, I. *J. Am. Chem. Soc.* **2005**, *127* (4), 1078−1079.
(31) Sirringhaus, H.; Wilson, R. J.; Friend, R. H.; Inbasekaran, M.; Wu, W.; Woo, E. P.; Grell, M.; Bradley, D. D. C. *Appl. Phys. Lett.* **2000**, *77* (3), 406−408.
(32) McCulloch, I.; Bailey, C.; Giles, M.; Heeney, M.; Love, I.; Shkunov, M.; Sparrowe, D.; Tierney, S. *Chem. Mater.* **2005**, *17* (6), 1381−1385.
(33) Hu, X. L.; Shi, M. M.; Chen, J. A.; Zuo, L. J.; Fu, L.; Liu, Y. J.; Chen, H. Z. *Macromol. Rapid Commun.* **2011**, *32* (6), 506−511.
(34) Murphy, A. R.; Liu, J. S.; Luscombe, C.; Kavulak, D.; Frechet, J. M. J.; Kline, R. J.; McGehee, M. D. *Chem. Mater.* **2005**, *17* (20), 4892−4899.
(35) Pomerantz, M.; Cheng, Y.; Kasim, R. K.; Elsenbaumer, R. L. *J. Mater. Chem.* **1999**, *9* (9), 2155−2163.
(36) Wang, C.; Kim, F. S.; Ren, G. Q.; Xu, Y. Q.; Pang, Y.; Jenekhe, S. A.; Jia, L. *J. Polym. Sci., Part A: Polym. Chem.* **2010**, *48* (21), 4681−4690.
(37) Kim, Y. G.; Walker, J.; Samuelson, L. A.; Kumar, J. *Nano Lett.* **2003**, *3* (4), 523−525.
(38) Liu, J. S.; Kadnikova, E. N.; Liu, Y. X.; McGehee, M. D.; Frechet, J. M. J. *J. Am. Chem. Soc.* **2004**, *126* (31), 9486−9487.
(39) Nazeeruddin, M. K.; Kay, A.; Rodicio, I.; Humphrybaker, R.; Muller, E.; Liska, P.; Vlachopoulos, N.; Gratzel, M. *J. Am. Chem. Soc.* **1993**, *115* (14), 6382−6390.
(40) van Hal, P. A.; Wienk, M. M.; Kroon, J. M.; Janssen, R. A. J. *J. Mater. Chem.* **2003**, *13* (5), 1054−1057.
(41) Vallat, P.; Lamps, J. P.; Schosseler, F.; Rawiso, M.; Catala, J. M. *Macromolecules* **2007**, *40* (7), 2600−2602.
(42) Loewe, R. S.; Ewbank, P. C.; Liu, J. S.; Zhai, L.; McCullough, R. D. *Macromolecules* **2001**, *34* (13), 4324−4333.
(43) Yokozawa, T.; Adachi, I.; Miyakoshi, R.; Yokoyama, A. *High Perform. Polym.* **2007**, *19* (5−6), 684−699.
(44) Iovu, M. C.; Sheina, E. E.; Gil, R. R.; McCullough, R. D. *Macromolecules* **2005**, *38* (21), 8649−8656.
(45) Trznadel, M.; Pron, A.; Zagorska, M. *Macromolecules* **1998**, *31* (15), 5051−5058.
(46) Wu, P. T.; Ren, G. Q.; Jenekhe, S. A. *Macromolecules* **2010**, *43* (7), 3306−3313.